JOURNAL OF GUIDANCE, CONTROL, AND DYNAMICS
Vol. 31, No. 6, November–December 2008

On-Orbit Identification of Inertia Properties of Spacecraft Using a Robotic Arm

Ou Ma* and Hung Dang†
New Mexico State University, Las Cruces, New Mexico 88003
and
Khanh Pham‡
U.S. Air Force Research Laboratory,
Kirtland Air Force Base, New Mexico 87117-5776

DOI: 10.2514/1.35188

This paper presents a robotics-based method for on-orbit identification of inertia properties of spacecraft. The method makes use of an onboard robotic arm to change the inertia distribution of the spacecraft system. As a result of the inertia redistribution, the velocity of the spacecraft system will change correspondingly. Because the velocity change is measurable and the inertia redistribution of the robotic arm itself is precisely computable, the inertia parameters of the spacecraft body become the only unknown in the momentum equations and, hence, can be identified from the momentum equations of the spacecraft system. To treat the problem as a linear identification problem, it has to be solved in two steps. The first step is to identify the mass and mass center of the spacecraft; and the second step is to identify the inertia tensor of the spacecraft. The advantages of this method are 1) it does not consume fuel because a robotic subsystem is energized by solar power; 2) it requires measuring velocities only, but not accelerations and forces; and 3) it is not affected by internal forces, which are difficult to accurately measure. The paper investigates the sensitivity of the method with respect to different arm/spacecraft mass ratios, arm motion trajectories, and velocity-measurement errors.

Nomenclature

C = mass center of the spacecraft system that is also used as the origin of the orbital frame
C_R = mass center of the robotic arm
C_S = mass center of the spacecraft body
$\mathbf{c}_R$ = position vector of the mass center of the robot with respect to the mass center of the spacecraft system (from C to C_R)
$\dot{\mathbf{c}}_R$ = velocity vector of the mass center of the robot with respect to the orbital frame
$\mathbf{c}_S$ = position vector of the mass center of the spacecraft body with respect to the mass center of the spacecraft system (from C to C_S)
$\dot{\mathbf{c}}_S$ = velocity vector of the mass center of the spacecraft body with respect to the orbital frame
F_E = Earth frame that is an inertial frame originating at the center O_E of the earth
F_S = spacecraft frame that is fixed to the spacecraft body and originating at point O_S of the spacecraft body
F_0 = inertial frame
$\mathbf{h}_C$ = angular momentum vector of the spacecraft system with respect to its mass center C
$\mathbf{h}_C(0)$ = initial angular momentum of the spacecraft system
$\mathbf{I}_C$ = inertia tensor of the spacecraft system with respect to its mass center C
$\mathbf{I}_R$ = inertia tensor of the robotic arm with respect to its mass center C_R
$\mathbf{I}_{R,C}$ = inertia tensor of the robot with respect to the mass center of the spacecraft system (i.e., C)
$\mathbf{I}_S$ = inertia tensor of the spacecraft body with respect to its own mass center C_S
$\mathbf{I}_{S,C}$ = inertia tensor of the spacecraft body with respect to the mass center of the spacecraft system
m_R = mass of the robotic arm
m_S = mass of the spacecraft body
n = total number of links of the robotic arm
l = total number of velocity measurements in an identification procedure
O_S = origin of the spacecraft frame, which is a fixed point on the spacecraft body
$\mathbf{p}_C$ = linear momentum vector of the spacecraft system with respect to its mass center C
$\mathbf{p}_C(0)$ = initial linear momentum of the spacecraft system
$\mathbf{v}_C$ = linear velocity vector of the mass center C of the spacecraft system
$\mathbf{v}_{C_R}$ = linear velocity vector of the mass center C_R of the robot
$\mathbf{v}_{C_S}$ = linear velocity vector of the mass center C_S of the spacecraft body
$\mathbf{v}_S$ = linear velocity of the origin O_S of the spacecraft frame F_S
$\boldsymbol{\rho}_C$ = position vector of the mass center of the spacecraft system with respect to the origin of the spacecraft frame (from O_S to C)
$\boldsymbol{\rho}_R$ = position vector of the mass center of the robot with respect to the origin of the spacecraft frame (from O_S to C_R)
$\boldsymbol{\rho}_S$ = position vector of the mass center of the spacecraft body with respect to the origin of the spacecraft frame (from O_S to C_S)
$\Sigma\mathbf{f}_i$ = resultant external force vector exerted on the spacecraft system

Presented as Paper 6815 at the AIAA Guidance, Navigation, and Control Conference, Hilton Head, SC, 20–23 August 2007; received 18 October 2007; accepted for publication 22 May 2008. Copyright © 2008 by the American Institute of Aeronautics and Astronautics, Inc. All rights reserved. Copies of this paper may be made for personal or internal use, on condition that the copier pay the $10.00 per-copy fee to the Copyright Clearance Center, Inc., 222 Rosewood Drive, Danvers, MA 01923; include the code 0731-5090/08 $10.00 in correspondence with the CCC.

*Ph.D. and Associate Professor, Department of Mechanical and Aerospace Engineering; oma@nmsu.edu. Senior Member AIAA.
†Ph.D. Candidate, Department of Electrical and Computer Engineering.
‡Ph.D. and Aerospace Engineer, Spacecraft Component Technology Branch; Khanh.Pham@kirtland.af.mil. Member AIAA.

$\Sigma\boldsymbol{\tau}_i$ = resultant external torque vector exerted on the spacecraft system
$\boldsymbol{\omega}$ = angular velocity vector of the spacecraft system when the robot is locked in a specific configuration without relative motion with respect to the spacecraft
$\boldsymbol{\omega}_S$ = angular velocity vector of the spacecraft body
$\mathbf{1}$ = 3×3 identity matrix

I. Introduction

THE inertia properties of a spacecraft can change in orbit for many reasons, such as fuel consumption, hardware reconfiguration, payload deployment, capturing of a flyer, docking with a satellite, or some mechanical malfunctions (e.g., an unexpected deployment failure). The spacecraft's state estimator or control system needs to know the correct inertia parameters. For example, after a servicing spacecraft is docked to a target satellite for servicing, the active vehicle has to stabilize the compound two-vehicle system before a service job can be performed. Such a stabilization operation cannot be done optimally (in the sense of fuel economy, time efficiency, dynamic impact, etc.) if the active vehicle does not have the knowledge of the inertia properties of the new compound system.

Robotics-based (unmanned) satellite on-orbit servicing has been gaining increasing attention in the international space community. Several technology developments and demonstration missions have been either done recently or are planned for the near future around the world [1–6]. There are significant advantages to having a robotics-based mission to rescue or service a satellite in space for economic or emergency purposes. However, enabling technologies required for autonomous on-orbit servicing have not all been mature. Many research activities are still going on around the world. Japan completed an on-orbit technology demonstration mission ETS-7 in 1999 [1]. In that mission, docking and simple robotic operations were tested under the condition that all details of the spacecraft are perfectly known. The Defense Advanced Research Projects Agency and the U.S. Air Force developed a technology demonstration mission through the Orbital Express Program [2], and the mission was successfully completed in 2007. In that mission, more advanced robotic and docking operations, including capturing and refuelling, were exercised on orbit. However, the servicing spacecraft still perfectly knew the serviced satellite, and the relative motion between the two spacecraft was still gentle. Germany, Russia, and Canada are also jointly developing a spacecraft rescue-and-service mission called TECSAS (Technology Satellite for Demonstration and Verification of Space Systems) [4,5]. In that mission, the rescuing spacecraft will be launched two years after the target satellite, which will have a slight tumbling motion during the capture operation. In that case, identification of the target satellite's inertia properties may become desirable. Future on-orbit rescue-and-service missions will face more aggressive scenarios, such as to capture a tumbling satellite or other space object with unknown inertia. In such a mission, a quick identification of the inertia properties of the postcapture compound system will be the key for the postcapture stabilization and subsequent operations.

There exist several methods for on-orbit identification of inertia properties [7–13]. Although they are different in details, most of them (i.e., [7–12]) use the same fundamental approach, which is based on the Newton–Euler equations of motion or referred to as propulsion-based methods. To estimate the unknown inertia properties from the equations of motion, one can convert the equations into a regression form and then apply the least-squares technique or other filtering techniques to solve for the unknown mass, position vector of the mass center, and inertia tensor (also called inertia matrix) of the spacecraft. It is easy to understand from the equations of motion that such an approach requires measuring not only the velocities but also the accelerations and the fired thrust forces of the spacecraft. The procedure is roughly illustrated in Fig. 1.

Precisely measuring the time history of the magnitude and direction of each thrust force is difficult. The preceding outlined force-based approach is basically followed in [7–10], and [11,12]

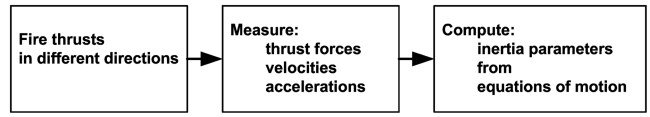

Fig. 1 Procedure of force-based approach for on-orbit identification of inertia properties.

smartly improved the approach by eliminating the nonlinear inertia moment $\boldsymbol{\omega} \times \mathbf{I}\boldsymbol{\omega}$ from the regression equation by premultiplying $\boldsymbol{\omega}$ with each term of the Euler equation. This means that, instead of using the vector form of the Euler equation, a specific projection perpendicular to the angular velocity vector $\boldsymbol{\omega}$ is used to form the regression system for identification. This improves the estimation process, but the method still requires known external excitations (such as firing thrusts). Without external excitations, the method works only for a rotating spacecraft with the assumption that the initial rotational kinetic energy is already known. The work reported in [12] also takes into account of the gravity-gradient torques on the identification results.

The only published work that is fundamentally different from the preceding force-based approach is reported in [13]. That approach is based on the principle of conservation of angular momentum and, thus, is a momentum-based approach. The method uses momentum wheels and the associated attitude control system to perform a set of attitude maneuvers and then measures the corresponding attitude, angular velocity, and wheel momentum for the identification process. Because the motion (or degrees of freedom) of a momentum wheel is limited and the method is based on angular momentum equation only, it cannot identify the mass and position of the mass center of the spacecraft. Momentum-wheel-based methods have the advantage of no fuel consumption.

This paper presents a method of using an onboard robotic arm to assist the identification of the inertia properties of spacecraft. The method was originally proposed in [14] without detailed performance investigation. The method makes use of a robotic arm to change the inertia distribution of the spacecraft system. As a result of the inertia redistribution, the velocity of the spacecraft system will change correspondingly. Because the velocity change is measurable and the inertia change of the robotic arm is precisely computable, the inertia parameters of the spacecraft body become the only unknowns in the momentum equations and, hence, can be identified. The procedure is illustrated in Fig. 2.

Identification of the inertia properties of spacecraft using an onboard robotic arm is a new approach. The closest works published in the literature would be [15,16], where the authors proposed methods of identifying the inertia properties of a payload handled by a robotic arm in space. The two references discussed both momentum-based and force-based methods for identification of the inertia parameters of the robot's payload. The main difference between their works and the work presented in this paper is that in their problems the payload of the robot is unknown, whereas in this paper the flying base of the robot is unknown. The method proposed in this paper has the following pros and cons:

1) Because the robotic arm is energized by solar energy, this method does not consume any fuel from the spacecraft. On the contrary, the propulsion-based methods have to consume fuel.

2) The method is based on the conservation-of-momentum principle and, thus, requires only velocity data. Propulsion-based methods require velocity, acceleration, and force data because they are based on the equations of motion. Also, force and acceleration data are noisier than velocity data.

3) Because the method is based on momentum conservation, any unknown internal forces in the system will not affect the identification results. On the contrary, unmodeled forces (e.g.,

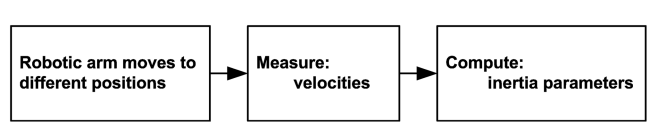

Fig. 2 Procedure of the approach for on-orbit identification of inertia properties.

friction forces) may corrupt the identification results of a method based on the equations of motion.

4) Because the method is based on the momentum-conservation law, the identification results will not be affected by how the robotic arm moves from one configuration to another. It requires measuring velocities only in several arm configurations, and, thus, each measurement can be done after the arm is settled in a new configuration.

5) The method requires a robotic arm onboard the spacecraft. However, this will likely be the case for a spacecraft designed for servicing a satellite in orbit.

6) The method requires an accurate kinematics model of the robot. This is usually available for a space robot because, for any space robot, high-fidelity modelling and simulation have already become mandatory in the design and development cycle.

The rest of the paper is organized as follows: Sec. II describes the formulation and procedure of the identification method; Sec. III presents the results of a simulation study; Sec. IV provides schemes for quantitatively estimate the identification error; and the paper is concluded in Sec. V.

II. Methodology

This section will discuss the formulation and solution procedure of the proposed inertia identification method in detail.

A. Basic Definitions

To facilitate the development and discussion of the formulation and simulation results, we define a few basic terms as follows (referring to Figs. 3 and 4). The *robot* or *robotic arm* is the physical arm starting from the first joint of the robot to the end effector (i.e., the tip) of the robot. The *spacecraft body* or *spacecraft* is the physical spacecraft excluding the robotic arm. The *spacecraft system* is the physical spacecraft including the robotic arm.

In this paper, whenever we mention the inertia properties of the spacecraft, we mean the mass, location of the mass center, and inertia tensor of the spacecraft body (not including these of the robotic arm), represented in the spacecraft frame.

Based on the definition of mass centers and referring to Fig. 4, we have the following identities:

$$m_S\mathbf{c}_S + m_R\mathbf{c}_R = \mathbf{0} \quad \text{or} \quad \mathbf{c}_R = -\frac{m_S}{m_R}\mathbf{c}_S$$
$$\boldsymbol{\rho}_C = \frac{m_S\boldsymbol{\rho}_S + m_R\boldsymbol{\rho}_R}{m_S + m_R} \tag{1}$$

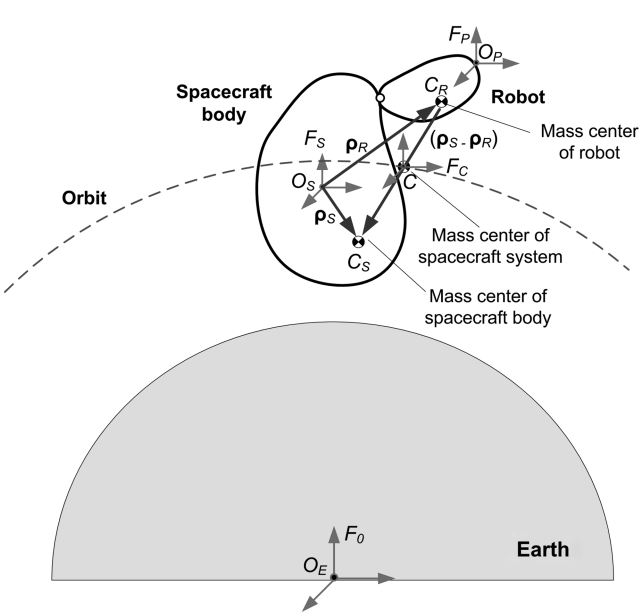

Fig. 3 Illustration of the coordinate system for dynamics modeling.

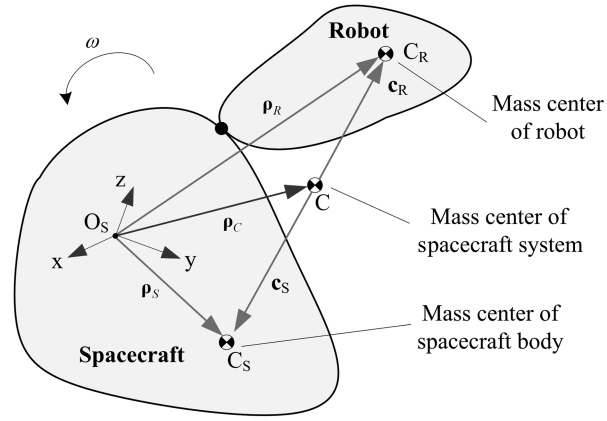

Fig. 4 Mass centers of the robotic arm, the spacecraft body, and the spacecraft system.

from which, we can further derive

$$\mathbf{c}_S = \boldsymbol{\rho}_S - \boldsymbol{\rho}_C = \frac{m_R}{m_S + m_R}(\boldsymbol{\rho}_S - \boldsymbol{\rho}_R)$$
$$\mathbf{c}_R = \boldsymbol{\rho}_R - \boldsymbol{\rho}_C = \frac{m_S}{m_S + m_R}(\boldsymbol{\rho}_R - \boldsymbol{\rho}_S)$$
$$\begin{aligned}\mathbf{I}_C &= \mathbf{I}_S + m_S\left[\left(\mathbf{c}_S^T\mathbf{c}_S\right)\mathbf{1} - \mathbf{c}_S\mathbf{c}_S^T\right] + \mathbf{I}_R \\ &\quad + m_R\left[\left(\mathbf{c}_R^T\mathbf{c}_R\right)\mathbf{1} - \mathbf{c}_R\mathbf{c}_R^T\right] = \mathbf{I}_S + \mathbf{I}_R \\ &\quad + \frac{m_S m_R}{m_S + m_R}((\boldsymbol{\rho}_S - \boldsymbol{\rho}_R)^T(\boldsymbol{\rho}_S - \boldsymbol{\rho}_R)\mathbf{1} - (\boldsymbol{\rho}_S - \boldsymbol{\rho}_R)(\boldsymbol{\rho}_S - \boldsymbol{\rho}_R)^T)\end{aligned} \tag{2}$$

Moreover, when the robot is locked in a configuration without relative motion with respect to the spacecraft, we have

$$\mathbf{v}_C = \mathbf{v}_S + \boldsymbol{\omega}_S \times \boldsymbol{\rho}_C, \qquad \mathbf{v}_{C_S} = \dot{\mathbf{c}}_S = \mathbf{v}_S + \boldsymbol{\omega}_S \times \boldsymbol{\rho}_S$$
$$\mathbf{v}_{C_R} = \dot{\mathbf{c}}_R = \mathbf{v}_S + \boldsymbol{\omega}_S \times \boldsymbol{\rho}_R \tag{3}$$

Then, the attitude dynamics equation of the spacecraft system is

$$\frac{d\mathbf{h}_C}{dt} = \frac{d(\mathbf{I}_C\boldsymbol{\omega})}{dt} = \Sigma\boldsymbol{\tau} + \Sigma(\boldsymbol{\rho}_i \times \mathbf{f}_i) \tag{4}$$

which can be rewritten in the form of

$$\mathbf{h}_C = \mathbf{I}_C\boldsymbol{\omega} = \mathbf{h}_C(0) + \int_0^t [\Sigma\boldsymbol{\tau} + \Sigma(\boldsymbol{\rho}_i \times \mathbf{f}_i)]\mathrm{d}t \tag{5}$$

Equations (4) and (5) can be represented either in the global frame or in a spacecraft fixed frame. The latter is more convenient for us because in the spacecraft fixed frame the unknown inertia parameters are constant.

The following is an important identity that will be repeatedly used in the derivation of the formulation:

$$\boldsymbol{\rho} \times (\boldsymbol{\omega} \times \boldsymbol{\rho}) = (\boldsymbol{\rho}^T\boldsymbol{\rho})\boldsymbol{\omega} - (\boldsymbol{\rho}^T\boldsymbol{\omega})\boldsymbol{\rho} = [(\boldsymbol{\rho}^T\boldsymbol{\rho})\mathbf{1} - \boldsymbol{\rho}\boldsymbol{\rho}^T]\boldsymbol{\omega} \tag{6}$$

B. Identification Method

Before describing the detailed identification formulation, we define the assumptions on which the formulation is derived:

1) There are no external forces and torques exerting on the spacecraft system.

2) Both the linear and angular velocities of the spacecraft are known (measured or estimated from other known data).

3) The configuration of the robotic arm is known (measured or derived from other known data).

The first assumption means that the spacecraft is freely floating in an orbit and the gravity-gradient effect is ignored. Because there are

no external forces and torques applied to the spacecraft, the linear and angular momentums are conserved, namely

$$\mathbf{p}_C = \mathbf{p}_C(0), \qquad \mathbf{h}_C = \mathbf{h}_C(0) \tag{7}$$

where $\mathbf{p}_C(0)$ and $\mathbf{h}_C(0)$ are the initial linear and angular momentums of the spacecraft system, respectively. Equation (7) can be expressed in detail as

$$\begin{aligned}\mathbf{p}_C &= \mathbf{p}_{S,C} + \mathbf{p}_{R,C} = m_S\dot{\mathbf{c}}_S + m_R\dot{\mathbf{c}}_R = m_S(\mathbf{v}_S + \boldsymbol{\omega}_S \times \boldsymbol{\rho}_S) \\ &\quad + m_R(\mathbf{v}_S + \boldsymbol{\omega}_S \times \boldsymbol{\rho}_R) = \mathbf{p}_C(0)\end{aligned} \tag{8}$$

$$\begin{aligned}\mathbf{h}_C &= \mathbf{h}_{S,C} + \mathbf{h}_{R,C} = \mathbf{I}_S\boldsymbol{\omega} + \mathbf{c}_S \times m_S\dot{\mathbf{c}}_S + \mathbf{I}_R\boldsymbol{\omega}_S + \mathbf{c}_R \times m_R\dot{\mathbf{c}}_R \\ &= \Bigg[\mathbf{I}_S + \mathbf{I}_R + \frac{m_S m_R}{m_S + m_R}((\boldsymbol{\rho}_S - \boldsymbol{\rho}_R)^T(\boldsymbol{\rho}_S - \boldsymbol{\rho}_R)\mathbf{1} \\ &\quad - (\boldsymbol{\rho}_S - \boldsymbol{\rho}_R)(\boldsymbol{\rho}_S - \boldsymbol{\rho}_R)^T)\Bigg]\boldsymbol{\omega}_S = \mathbf{I}_C\boldsymbol{\omega}_S = \mathbf{h}_C(0)\end{aligned} \tag{9}$$

Note that the unknown inertia variables m_S and $\boldsymbol{\rho}_S$ appear nonlinearly in both equations. Therefore, linear identification techniques can not be applied. We can overcome the nonlinearity problem by solving the problem in two separate steps. The first step is to identify the mass and mass center, and the second step is to find the inertia tensor.

1. *Step 1: Identification of Mass m_S and Position of Mass Center $\boldsymbol{\rho}_S$*

Rewrite Eq. (8) as

$$\frac{m_R}{m_S}\left(\mathbf{v}_S + \boldsymbol{\omega}_S \times \boldsymbol{\rho}_R - \frac{\mathbf{p}_C(0)}{m_R}\right) + \boldsymbol{\omega}_S \times \boldsymbol{\rho}_S = -\mathbf{v}_S \tag{10}$$

which is linear in terms of the unknown terms m_R/m_S and $\boldsymbol{\rho}_S$.

By moving the arm into a sequence of different configurations, say, $C_1, C_2, \ldots, C_m$, and measuring the resulting linear and angular velocities of the spacecraft body, $(\mathbf{v}_{S1}, \boldsymbol{\omega}_{S1})$, $(\mathbf{v}_{S2}, \boldsymbol{\omega}_{S2}), \ldots, (\mathbf{v}_{Sm}, \boldsymbol{\omega}_{Sm})$, we can construct a large system of linear regression equations in terms of the unknowns m_R/m_S and $\boldsymbol{\rho}_S$. Then, solve these two unknowns from the regression equations using the least-squares method. Because m_R is a known constant, we can find m_S easily after we have found the unknown term m_R/m_S. We have two options to write the linear regression equations depending on whether the initial linear momentum $\mathbf{p}_C(0)$ is known or not. The two options are described as follows:

Option 1: The initial linear momentum $\mathbf{p}_C(0)$ is known.

If the initial momentum of the system is known, then we can construct the linear regression equations as follows:

$$\mathbf{A}\mathbf{x} = \mathbf{b} \tag{11}$$

where

$$\mathbf{x} \equiv \begin{bmatrix} m_R/m_S \\ \boldsymbol{\rho}_S \end{bmatrix}, \qquad \mathbf{A} \equiv \begin{bmatrix} \mathbf{A}_1 \\ \vdots \\ \mathbf{A}_l \end{bmatrix}, \qquad \mathbf{b} \equiv \begin{bmatrix} \mathbf{b}_1 \\ \vdots \\ \mathbf{b}_l \end{bmatrix} \tag{12}$$

and

$$\begin{gathered}\mathbf{A}_k = \left[\left(\mathbf{v}_{Sk} + \boldsymbol{\omega}_{Sk} \times \boldsymbol{\rho}_{Rk} - \frac{\mathbf{p}_C(0)}{m_R}\right) \quad \boldsymbol{\Omega}_k\right], \qquad \mathbf{b}_k = -\mathbf{v}_{Sk} \\ \boldsymbol{\Omega}_k \equiv \boldsymbol{\omega}_{Sk}^{\times} = \begin{bmatrix} 0 & -\omega_{Sk}(3) & \omega_{Sk}(2) \\ \omega_{Sk}(3) & 0 & -\omega_{Sk}(1) \\ -\omega_{Sk}(2) & \omega_{Sk}(1) & 0 \end{bmatrix} \qquad k = 1, 2, \ldots, l\end{gathered} \tag{13}$$

where $\mathbf{v}_{Sk}$ and $\boldsymbol{\omega}_{Sk}$ are linear and angular velocities of the spacecraft body measured at the kth configuration of the robotic arm; l is the total number of configurations for velocity measurements. Vector $\boldsymbol{\rho}_{Rk}$ is the position of the mass center of the entire robot when it is at the kth configuration, which can be computed (see Sec. II.C). Because the momentum of the system is conserved, the measurement of the velocities at each arm configuration can be done at any time after the arm made a configuration change. However, the measurement is better done after the arm is fully settled in a new configuration and the velocities to be measured reach a steady state (if they can reach a steady state) because a steady-state velocity can be measured more accurately than a transient velocity. This is particularly important if the robotic arm is flexible (elastic). If the spacecraft velocity does not reach a steady state after the arm settled in a new configuration, the transient velocities have to be measured and used for the identification.

Option 2: The initial linear momentum $\mathbf{p}_C(0)$ is unknown.

In this case, we need to eliminate the initial momentum from the momentum equations. This can be done by rewriting Eq. (8) as a momentum increment equation as follows:

$$\begin{aligned}\mathbf{p}_C - \mathbf{p}_C(0) &= m_S(\Delta\mathbf{v}_{Sk} + \Delta\boldsymbol{\omega}_{Sk} \times \boldsymbol{\rho}_S) \\ &\quad + m_R(\Delta\mathbf{v}_{Sk} + \Delta\boldsymbol{\omega}_{Sk} \times \boldsymbol{\rho}_{Rk} + \boldsymbol{\omega}_{S0} \times \Delta\boldsymbol{\rho}_{Rk}) = \mathbf{0}\end{aligned} \tag{14}$$

$\Delta\mathbf{v}_{Sk}$, $\Delta\boldsymbol{\omega}_{Sk}$, and $\Delta\boldsymbol{\rho}_{Rk}$ are the increments of the spacecraft linear velocity, the spacecraft angular velocity; the robot mass center from the initial time to the time when the robot is at the kth configuration; and $\boldsymbol{\omega}_{S0}$ is the initial angular velocity of the spacecraft. Notice that the resulting equation no longer has the initial momentum term, and, hence, we can form the following new linear regression equation:

$$\mathbf{A}\mathbf{x} = \mathbf{b} \tag{15}$$

where

$$\mathbf{x} \equiv \begin{bmatrix} m_R/m_S \\ \boldsymbol{\rho}_S \end{bmatrix}, \qquad \mathbf{A} \equiv \begin{bmatrix} \mathbf{A}_1 \\ \vdots \\ \mathbf{A}_l \end{bmatrix}, \qquad \mathbf{b} \equiv \begin{bmatrix} \mathbf{b}_1 \\ \vdots \\ \mathbf{b}_l \end{bmatrix} \tag{16}$$

and

$$\begin{gathered}\mathbf{A}_k = [(\Delta\mathbf{v}_{Sk} + \Delta\boldsymbol{\omega}_{Sk} \times \boldsymbol{\rho}_{Rk} + \boldsymbol{\omega}_{S0} \times \Delta\boldsymbol{\rho}_{Rk}) \quad \boldsymbol{\Omega}_k] \\ \mathbf{b}_k = -\Delta\mathbf{v}_{Sk} \\ \boldsymbol{\Omega}_k \equiv \Delta\boldsymbol{\omega}_{Sk}^{\times} = \begin{bmatrix} 0 & -\Delta\omega_{Sk}(3) & \Delta\omega_{Sk}(2) \\ \Delta\omega_{Sk}(3) & 0 & -\Delta\omega_{Sk}(1) \\ -\Delta\omega_{Sk}(2) & \Delta\omega_{Sk}(1) & 0 \end{bmatrix} \\ \Delta\boldsymbol{\omega}_{Sk} = \boldsymbol{\omega}_{Sk} - \boldsymbol{\omega}_{S0}, \qquad \Delta\boldsymbol{\rho}_{Rk} = \boldsymbol{\rho}_{Rk} - \boldsymbol{\rho}_{R0}, \qquad k = 1, 2, \ldots, l\end{gathered} \tag{17}$$

Note that using the relative velocities $\Delta\mathbf{v}_{Sk}$ and $\Delta\boldsymbol{\omega}_{Sk}$ for identification has two advantages in comparison to using the absolute velocities $\mathbf{v}_{Sk}$ and $\boldsymbol{\omega}_{Sk}$: 1) the relative velocities can be easily obtained from integrating accelerometer data and 2) relative velocities have less measurement bias (i.e., systematic errors). The disadvantage of using the relative velocities is that it is more sensitive to measurement noise due to a lower signal-to-noise ratio, as will be discussed in Sec. III.D.

2. *Step 2: Identification of Inertia Tensor $\mathbf{I}_S$*

After the completion of step 1, the inertia variables m_S and $\boldsymbol{\rho}_S$ become known. We can then identify the components of the inertia tensor $\mathbf{I}_S$. Again, there are two options depending on whether the initial angularf momentum is known or not.

Option 1: The initial angular momentum $\mathbf{h}_C(0)$ is known.

Based on Eq. (9), we can construct the following linear regression equation:

$$\mathbf{B}\mathbf{y} = \mathbf{c} \tag{18}$$

where

$$\mathbf{y} \equiv \begin{bmatrix} I_S(1,1) \\ I_S(2,2) \\ I_S(3,3) \\ I_S(1,2) \\ I_S(1,3) \\ I_S(2,3) \end{bmatrix}, \qquad \mathbf{B} \equiv \begin{bmatrix} \mathbf{B}_1 \\ \vdots \\ \mathbf{B}_l \end{bmatrix}, \qquad \mathbf{c} \equiv \begin{bmatrix} \mathbf{c}_1 \\ \vdots \\ \mathbf{c}_l \end{bmatrix} \tag{19}$$

and

$$\mathbf{B}_k = \begin{bmatrix} \Delta\omega_{Sk}(1) & 0 & 0 & \Delta\omega_{Sk}(2) & \Delta\omega_{Sk}(3) & 0 \\ 0 & \Delta\omega_{Sk}(2) & 0 & \Delta\omega_{Sk}(1) & 0 & \Delta\omega_{Sk}(3) \\ 0 & 0 & \Delta\omega_{Sk}(3) & 0 & \Delta\omega_{Sk}(1) & \Delta\omega_{Sk}(2) \end{bmatrix}$$

$$\mathbf{c}_k = -\left(\mathbf{I}_{Rk} + \frac{m_R m_S}{m_S + m_R}\mathbf{T}_k\right)\Delta\boldsymbol{\omega}_{Sk} - \left[\mathbf{I}_{Rk} - \mathbf{I}_{R0} + \frac{m_R m_S}{m_S + m_R}(\mathbf{T}_k - \mathbf{T}_0)\right]\boldsymbol{\omega}_{S0} \tag{24}$$

$$\mathbf{T}_k = (\boldsymbol{\rho}_S - \boldsymbol{\rho}_{Rk})^T(\boldsymbol{\rho}_S - \boldsymbol{\rho}_{Rk})\mathbf{1} - (\boldsymbol{\rho}_S - \boldsymbol{\rho}_{Rk})(\boldsymbol{\rho}_S - \boldsymbol{\rho}_{Rk})^T$$

$$\mathbf{T}_0 = (\boldsymbol{\rho}_S - \boldsymbol{\rho}_{R0})^T(\boldsymbol{\rho}_S - \boldsymbol{\rho}_{R0})\mathbf{1} - (\boldsymbol{\rho}_S - \boldsymbol{\rho}_{R0})(\boldsymbol{\rho}_S - \boldsymbol{\rho}_{R0})^T, \qquad k = 1, 2, \cdots, m$$

$$\mathbf{B}_k = \begin{bmatrix} \omega_{Sk}(1) & 0 & 0 & \omega_{Sk}(2) & \omega_{Sk}(3) & 0 \\ 0 & \omega_{Sk}(2) & 0 & \omega_{Sk}(1) & 0 & \omega_{Sk}(3) \\ 0 & 0 & \omega_{Sk}(3) & 0 & \omega_{Sk}(1) & \omega_{Sk}(2) \end{bmatrix}$$

$$\mathbf{c}_k = \mathbf{h}_C(0) - \mathbf{I}_{Rk}\boldsymbol{\omega}_{Sk} - \frac{m_R m_S}{m_S + m_R}(\boldsymbol{\rho}_S - \boldsymbol{\rho}_{Rk}) \times [\boldsymbol{\omega}_{Sk} \times (\boldsymbol{\rho}_S - \boldsymbol{\rho}_{Rk})], \qquad k = 1, 2, \ldots, l \tag{20}$$

where $\boldsymbol{\omega}_{Sk}$ is the angular velocity of the spacecraft body measured at the kth configuration of the robotic arm. Terms $\boldsymbol{\rho}_{Rk}$ and $\mathbf{I}_{Rk}$ are the position of the mass center and the centroid inertia tensor of the entire robot when it is at the kth configuration, which can be computed from the robot model (see Sec. II.C). The term $I_S(i, j)$ is the (i, j)th component of the inertia tensor $\mathbf{I}_S$, which is represented in the spacecraft frame.

Option 2: The initial angular momentum $\mathbf{h}_C(0)$ is unknown.

In this case, we need to eliminate the initial momentum. This can be done by rewriting Eq. (9) into a momentum increment equation as follows:

$$\begin{aligned} \mathbf{h}_C - \mathbf{h}_C(0) &= \mathbf{I}_S\Delta\boldsymbol{\omega}_{Sk} \\ &+ \left[\mathbf{I}_{Rk} + \frac{m_R m_S}{m_S + m_R}((\boldsymbol{\rho}_S - \boldsymbol{\rho}_{Rk})^T(\boldsymbol{\rho}_S - \boldsymbol{\rho}_{Rk})\mathbf{1} \right. \\ &\left. - (\boldsymbol{\rho}_S - \boldsymbol{\rho}_{Rk})(\boldsymbol{\rho}_S - \boldsymbol{\rho}_{Rk})^T)\right]\Delta\boldsymbol{\omega}_{Sk} \\ &+ \left[\mathbf{I}_{Rk} - \mathbf{I}_{R0} + \frac{m_R m_S}{m_S + m_R}((\boldsymbol{\rho}_S - \boldsymbol{\rho}_{Rk})^T(\boldsymbol{\rho}_S - \boldsymbol{\rho}_{Rk})\mathbf{1} \right. \\ &\left. - (\boldsymbol{\rho}_S - \boldsymbol{\rho}_{Rk})(\boldsymbol{\rho}_S - \boldsymbol{\rho}_{Rk})^T)\right]\boldsymbol{\omega}_{S0} \\ &- \frac{m_R m_S}{m_S + m_R}((\boldsymbol{\rho}_S - \boldsymbol{\rho}_{R0})^T(\boldsymbol{\rho}_S - \boldsymbol{\rho}_{R0})\mathbf{1} \\ &- (\boldsymbol{\rho}_S - \boldsymbol{\rho}_{R0})(\boldsymbol{\rho}_S - \boldsymbol{\rho}_{R0})^T)\boldsymbol{\omega}_{S0} = \mathbf{0}, \qquad k = 1, 2, \cdots, l \end{aligned} \tag{21}$$

where $\Delta\boldsymbol{\omega}_{Sk} = \boldsymbol{\omega}_{Sk} - \boldsymbol{\omega}_{S0}$ is the increment of the angular velocity of the spacecraft body from the initial time to the time when the robotic arm is at the kth configuration. Hence, we can form the following new linear regression equation:

$$\mathbf{B}\mathbf{y} = \mathbf{c} \tag{22}$$

where

$$\mathbf{y} \equiv \begin{bmatrix} I_S(1,1) \\ I_S(2,2) \\ I_S(3,3) \\ I_S(1,2) \\ I_S(1,3) \\ I_S(2,3) \end{bmatrix}, \qquad \mathbf{B} \equiv \begin{bmatrix} \mathbf{B}_1 \\ \vdots \\ \mathbf{B}_l \end{bmatrix}, \qquad \mathbf{c} \equiv \begin{bmatrix} \mathbf{c}_1 \\ \vdots \\ \mathbf{c}_l \end{bmatrix} \tag{23}$$

The components of the unknown inertia tensor of the spacecraft can be found from the least-squares solution to the preceding linear equations. Note that, in the equations, the mass center $\boldsymbol{\rho}_{Rk}$ and the inertia tensor $\mathbf{I}_{Rk}$ of the robotic arm can be computed as described in Sec. II.C.

C. Inertia Tensor and Momentums of the Robotic Arm

Although the mass center and inertia tensor of the robot change with the motion of the robot, they can be precisely computed as long as the inertia properties of individual links of the robot and the configuration of the robot are known. This is not difficult because the configuration of the robot is fully controlled and known, and the inertia properties of individual links of a space robot are always known. Before we present the corresponding computational formulas, the following assumptions need to be emphasized:

1) The robot consists of n moveable links, which are articulated by n single-degree-of-freedom joint.

2) The mass of each link of the robot is constant and known.

3) The position of mass center and inertia tensor of each link of the robot are known. Note that these two items are constant when they are represented in the body-fixed frame associated with the link.

4) The configuration and motion of the robot with respect to the spacecraft body are known. This known information can be represented by the joint angles and joint rates of the robot.

The kinematics of the robotic arm is defined as shown in Fig. 5. By definition, the position of the mass center and the inertia tensor of the entire robot with respect to the spacecraft frame F_S can be computed as follows:

$$\boldsymbol{\rho}_R = \frac{\sum_{i=1}^n m_i\boldsymbol{\rho}_i}{\sum_{i=1}^n m_i} \quad \text{and} \quad \mathbf{I}_R = \sum_{i=1}^n \mathbf{I}_i \tag{25}$$

In Eq. (25) m_i is the mass of the ith link; $\boldsymbol{\rho}_i$ and $\mathbf{I}_i$ are, respectively, the position vector of the mass center and the inertia tensor of the ith link with respect to the origin of the spacecraft frame F_S and also represented in F_S. They can be computed using the following kinematic relations:

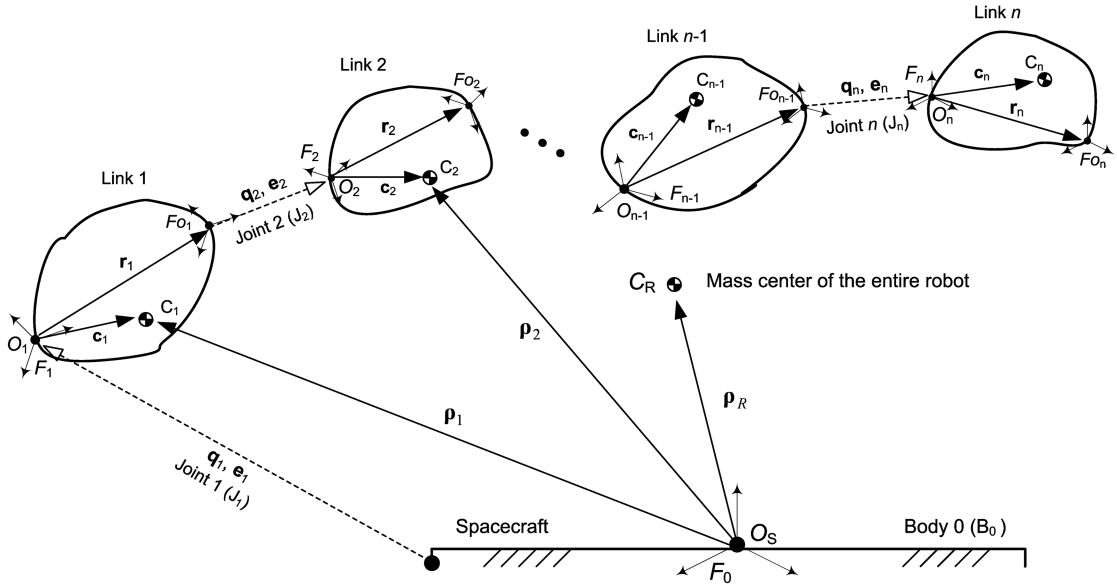

Notation:

$\mathbf{q}_i$ -- Relative displacements (state variable) of Joint i, expressed in Fo_{i-1} frame (the outboard frame of previous link).

$\mathbf{e}_i$ -- Relative angular displacements of Joint i (represented by Euler angles or quaternions), expressed in Fo_{i-1}.

$\mathbf{r}_i$ -- Intrabody vector of link i, expressed in F_i frame (the inboard frame of the ith link).

$\mathbf{c}_i$ -- Position vector of the center of mass (C_i) of link i with respect to Joint i, expressed in F_i frame.

Fig. 5 Kinematics notation of the robotic arm.

$$\mathbf{R}_i = \Pi_{k=1}^{i}\, {}^{k}\mathbf{R}_k, \qquad \boldsymbol{\rho}_i = \sum_{k=1}^{i} \mathbf{R}_k\, {}^{k}r_k + \mathbf{R}_i\, {}^{i}\mathbf{c}_i$$
$$\mathbf{I}_i = \mathbf{R}_i\, {}^{i}\mathbf{I}_i \mathbf{R}_i^T + m_i[(\boldsymbol{\rho}_i^T \boldsymbol{\rho}_i)\mathbf{1} - \boldsymbol{\rho}_i \boldsymbol{\rho}_i^T], \qquad i = 1, 2, \ldots, n \tag{26}$$

In the preceding equations, ${}^{i}\mathbf{c}_i$ and ${}^{i}\mathbf{I}_i$ are the known mass center and inertia tensor of the ith link with respect to the body-fixed frame F_i, and, therefore, their values will not change during the robot motion. Moreover, vector ${}^{i}\mathbf{r}_i$ and matrix ${}^{i}\mathbf{R}_i$ represent the relative position and orientation from the ith joint (or the ith body frame) to the $(i+1)$th joint or the tip of the arm, expressed in the ith body-fixed frame, and thus, they are constant too.

With the foregoing definitions, the linear and angular momentums of the entire robot, with respect to the origin of the spacecraft frame, can be computed as follows:

$$\mathbf{p}_R = \sum_{i=1}^{n} m_i \mathbf{v}_{ci} = \sum_{i=1}^{n} m_i \mathbf{v}_{ci}$$
$$\mathbf{h}_R = \sum_{k=1}^{i} (\mathbf{I}_i \boldsymbol{\omega}_i + \boldsymbol{\rho}_i \times m_i \mathbf{v}_{ci}) \tag{27}$$

where $\mathbf{v}_{ci}$ and $\boldsymbol{\omega}_i$ are, respectively, the linear velocity of the mass center and the angular velocity of the ith link of the robot, which can be computed from the known joint angles and rates using the following recursive formulas:

$$\mathbf{v}_{ci} = \mathbf{v}_{ci-1} + \boldsymbol{\omega}_{i-1} \times \mathbf{R}_{i-1}({}^{i-1}\mathbf{r}_{i-1} - {}^{i-1}\mathbf{c}_{i-1}) + \boldsymbol{\omega}_i \times \mathbf{R}_i\, {}^{i}\mathbf{c}_i$$
$$\boldsymbol{\omega}_i = \boldsymbol{\omega}_{i-1} + \mathbf{R}_i \begin{bmatrix} 0 \\ 0 \\ 1 \end{bmatrix} \dot{\theta}_i \quad \text{for } i = 1, 2, \ldots, n \tag{28}$$

In the preceding formulation $\mathbf{v}_{c0}$ and $\boldsymbol{\omega}_0$ are the linear and angular velocities of the base of the robot, which is the spacecraft body in this case. In Eq. (28), it is assumed that the joint axis of the ith joint is along the Z axis of the ith body-fixed frame and the joint is a revolute joint. For the formulation of a more general robot, one can refer to [17].

III. Simulation Study

The inertia identification method has been tested using computer simulations. In this section the simulation model and the findings from the simulation study are discussed.

A. Simulation Model

The dynamics model for the simulation study consists of a rigid spacecraft and a 6-DOF (degree-of-freedom) robotic arm. The kinematics of the system, represented by nine coordinate frames, are defined in Figs. 6 and 7. The spacecraft frame F_S is fixed at the geometric center O_S of the spacecraft body. The ith local coordinate frame of the robot is attached to the ith link, and originated at the ith joint of the robot ($i = 1, 2, \ldots, 6$). The frame will move with the ith link. The tip frame F_7 is attached to the tip of the end effector, as

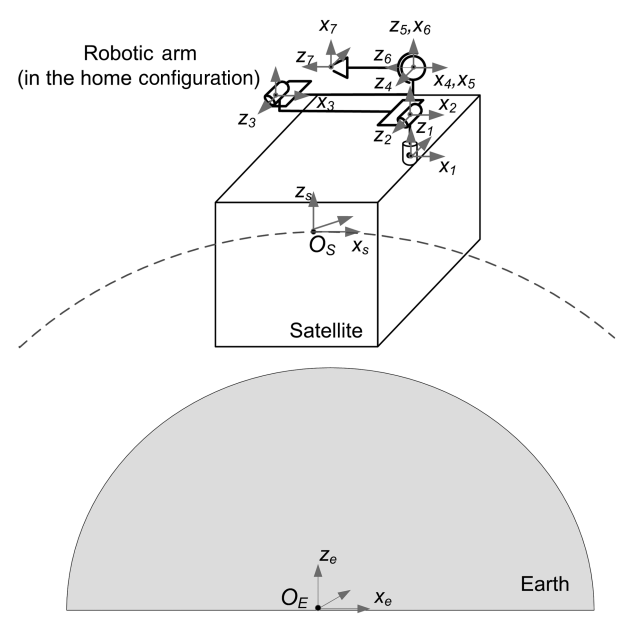

Fig. 6 Reference frames of the spacecraft and robotic arm in home configuration.

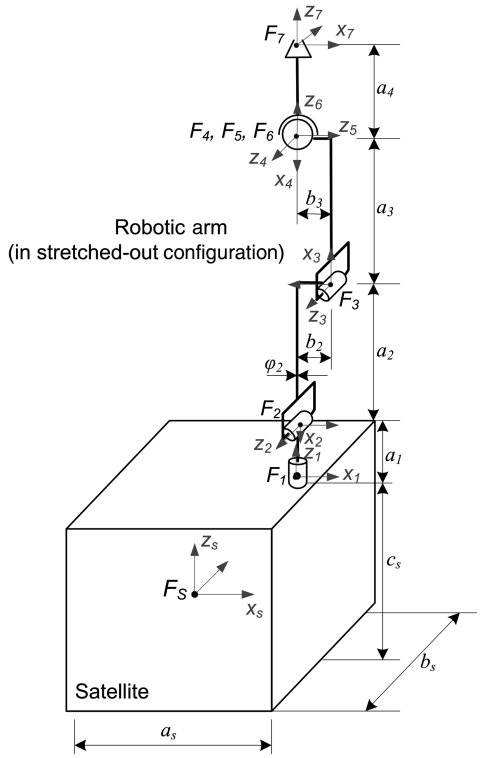

Fig. 7 Kinematic dimensions of the spacecraft and robotic arm.

shown in Figs. 6 and 7. The home configuration of the robot (where all the joint angles are zero) is shown in Fig. 6, namely, being completely folded to the top surface of the spacecraft body. The attaching point of the arm on the spacecraft body is also shown in Fig. 7. The kinematics and dynamics parameters of the arm implemented in the simulation model are listed in Table 1. The model has been implemented on MSC.ADAMS for dynamic simulation and on MATLAB for analysis.

Table 1 Kinematics and dynamics parameters of the spacecraft-arm system

Body	Parameters	Unit	Value
Spacecraft	a_s, b_s, c_s	m	1.0, 1.0, 1.0
	m_S	kg	1000.0
	${}^S\mathbf{c}_S$	m	$[0 \quad 0 \quad 0]^T$
	${}^S\mathbf{I}_S$	$\mathrm{kg \cdot m^2}$	diag(166.67, 166.67, 166.67)
Link 1	a_1, b_1, ϕ_1	m	0.2, 0.0, 0.025
	m_1	kg	7.597
	${}^1\mathbf{c}_1$	m	$[0 \quad 0 \quad a_1/2]^T$
	${}^1\mathbf{I}_1$	$\mathrm{kg \cdot m^2}$	Computed
Link 2	a_2, b_2, ϕ_2	m	1.0, 0.2, 0.025
	m_2	kg	34.885
	${}^2\mathbf{c}_2$	m	$[-a_2/2 \quad b_2/2 \quad 0]^T$
	${}^2\mathbf{I}_2$	$\mathrm{kg \cdot m^2}$	Computed
Link 3	a_3, b_3, ϕ_3	m	1.0, 0.2, 0.025
	m_3	kg	34.885
	${}^3\mathbf{c}_3$	m	$[a_3/2 \quad b_3/2 \quad 0]^T$
	${}^3\mathbf{I}_3$	$\mathrm{kg \cdot m^2}$	Computed
Link 4 (dummy link)	a_4, b_4, ϕ_4	m	0, 0, 0
	m_4	kg	0
	${}^4\mathbf{c}_4$	m	$[0 \quad 0 \quad 0]^T$
	${}^4\mathbf{I}_4$	$\mathrm{kg \cdot m^2}$	Computed
Link 5 (dummy link)	a_5, b_5, ϕ_5	m	0, 0, 0
	m_5	kg	0
	${}^5\mathbf{c}_5$	m	$[0 \quad 0 \quad 0]^T$
	${}^5\mathbf{I}_5$	$\mathrm{kg \cdot m^2}$	Computed
Link 6 (end effector)	a_6, b_6, ϕ_6	m	0.5, 0.0, 0.025
	m_6	kg	15.817
	${}^6\mathbf{c}_6$	m	$[0 \quad 0 \quad a_4/2]^T$
	${}^6\mathbf{I}_6$	$\mathrm{kg \cdot m^2}$	Computed

Note that the lengths of the fourth and fifth links of the arm are zero because the last three revolute joints are combined into a 3-DOF spherical joint.

B. Effect of Arm/Spacecraft Mass Ratio

Because the method is to use a robotic arm to redistribute the inertia of the spacecraft system so that the inertia properties of the spacecraft can be identified, the robotic arm has to have sufficiently large inertia to cause a measurable dynamic response of the spacecraft. To address this concern, many test examples were tried to see how the identification results vary with respect to the ratio of the arm mass over the spacecraft mass.

Simulation examples indicated that the identification accuracy is not as sensitive to the arm/spacecraft mass ratio as we originally thought. For example, the plot of identification errors vs different arm/spacecraft mass ratio is shown in Fig. 8. In this case, the arm is commanded to go along the first trajectory defined in Sec. III.C (see Figs. 9 and 10). Ten velocity measurements are taken at configurations equally separated along the trajectory. The spacecraft body is initially spinning about the Z axis at a rate of 5 deg/s. The plots indicate that, as long as the mass of the arm is not less than 5% of the spacecraft's mass, the resulting identification errors are almost similar regardless of how the arm mass compares to the spacecraft mass. A similar result is also seen in other examples, and, thus, it is representative. However, this observation is true only under the condition that all the velocity data can be perfectly measured. In other words, if the velocity data are perfect, then the arm/spacecraft mass ratio will cause almost no error in the identification result. The small error shown in Fig. 8 is the numerical error from the least-square solution of Eqs. (11), (15), (18), and (22).

Note that velocity measurements can never be perfectly accurate in reality. In fact, the mass ratio will affect the accuracy of velocity measurements by affecting the velocity's signal-to-noise ratio. If the arm is very light compared with the mass of the spacecraft body, the velocity variation resulting from the arm motion will be small and,

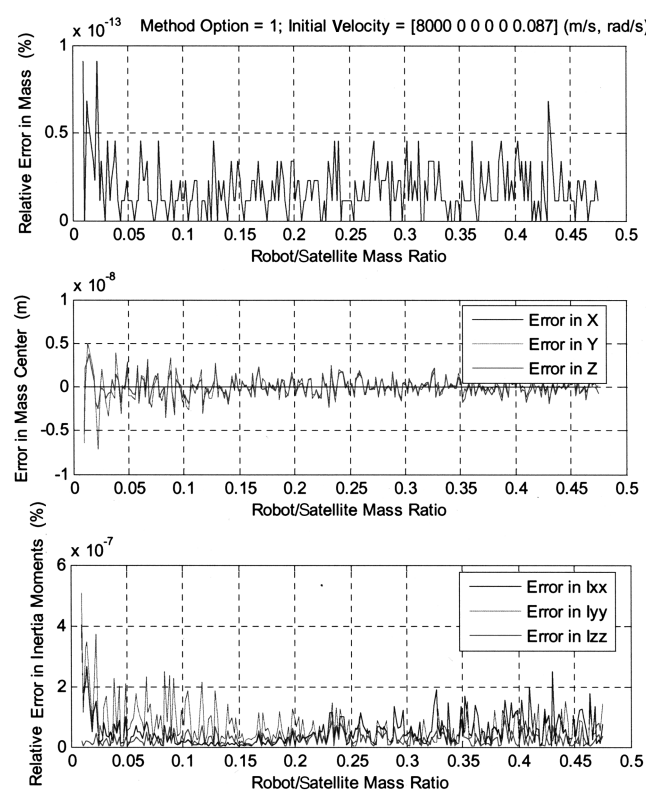

Fig. 8 Identification errors for different arm-spacecraft mass ratio. (Note that the error in the position of the mass center is represented by the absolute error because the mass center is located at the origin, and, thus, the relative error is undefined.)

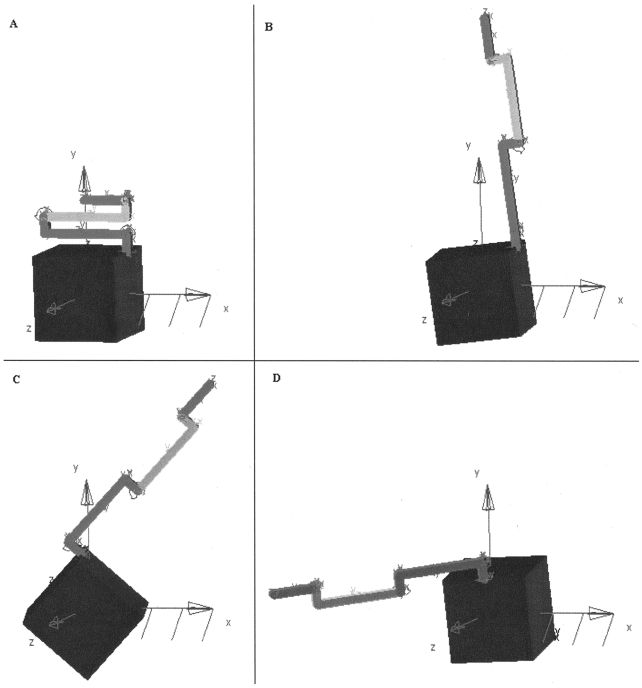

Fig. 9 Four special configurations (snapshots) of the arm taken from its first maneuvering trajectory.

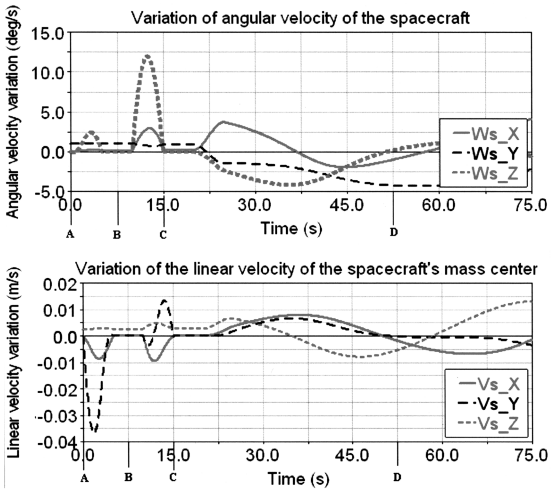

Fig. 10 Time histories of the velocity components of the spacecraft as the arm is moving along the first trajectory. (Note that the orbiting linear velocity is not included.)

thus, has a low signal-to-noise ratio, causing poor velocity data. As a result, the inaccurate velocity data may cause quite large identification errors. The effect of velocity errors on identification results will be discussed in Sec. III.D.

C. Effect of Arm Maneuvers

The method requires the robotic arm to move to different configurations to change the velocity of the spacecraft. It is then understandable that those configurations should be as different as possible to maximize the resulting new mass distribution and velocity variations. Moreover, to identify all the components of the inertia tensor, the velocity changes caused by the arm maneuvering must be in all directions. Therefore, the motion trajectory or path of the arm should span as large a space as possible. In our investigation, different arm trajectories were defined and tested by simulations. The following are two typical trajectories that we have tested.

Arm trajectory 1 (see Figs. 9 and 10) is a very general trajectory having a large motion span or maneuvering. The arm is originally at rest in its home configuration. It starts to stretch all the way upward, then swings down to the top plane of the spacecraft body while remaining fully stretched out, and then it rotates about the first joint (parallel to the Z axis of the spacecraft frame).

In responding to this arm maneuvering, the velocities of the spacecraft body will change. The time histories of the 3-D linear and angular velocities along the motion trajectory are plotted in Fig. 10. It is difficult to graphically represent the entire arm maneuvering on paper without a video representation. To get some idea about the arm trajectory, four special configurations of the arm chosen from the trajectory are shown in Fig. 9. The times corresponding to these four configurations are marked with A, B, C, and D on the plots (see Fig. 10). From the figures, we can clearly see that the spacecraft has different orientations corresponding to the four different arm configurations.

Note that the velocity components plotted in the figure are with respect to the orbit frame and, thus, they do not include the orbiting velocity. It is very difficult to include the orbiting motion in the dynamic simulation on ADAMS because the orbiting velocity is too large in comparison with the velocity variations due to the arm movement. However, the orbiting velocity has been included in the linear velocity of the spacecraft for our MATLAB-based simulation and analysis.

Figure 10 shows that all the six velocity components are changing during the time as the arm is moving along the specified trajectories. This indicates that the resulting identification problem is well defined. To have the best identification results, velocity data should be acquired at the points where the velocity components have large values.

Arm trajectory 2 (see Figs. 11 and 12) represents a simple maneuver of the arm, where the arm repeatedly stretches all the way up from its home configuration and then folds back to its home configuration. Two representative configurations of the arm are shown in Fig. 11, one of them is when the arm is fully folded down and the other is when the arm is fully stretched up. The time histories of all the components of the linear and angular velocities along the trajectory are plotted in Fig. 12. For the velocity plots, the initial angular velocity of the spacecraft was assumed to be 1 deg/s about the Y axis.

D. Sensitivity to Sensor Noise

Velocity measurements always have some errors due to sensor noise or other uncertainties. These errors will cause corresponding errors in the identification results. To assess the sensitivity to the

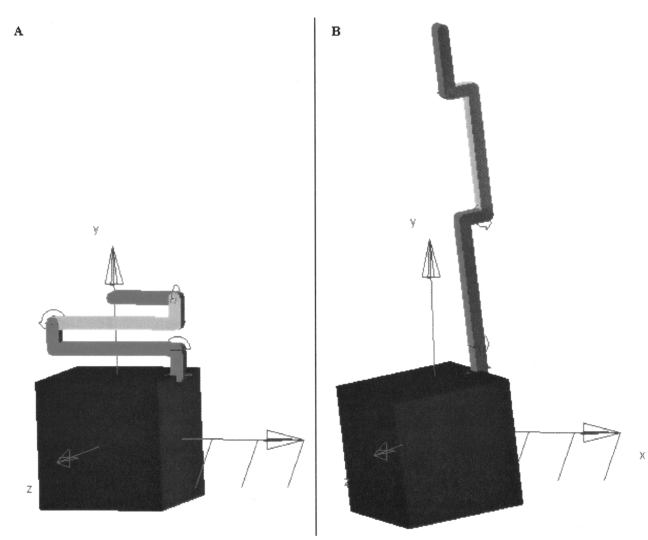

Fig. 11 Two special configurations of the arm picked from its second maneuvering trajectory.

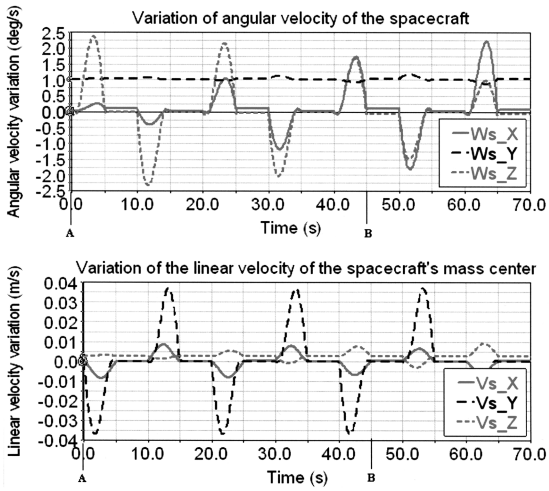

Fig. 12 Time histories of velocity components of the spacecraft as the arm is moving along the second trajectory. (Note that the orbiting linear velocity is not included).

sensor noise, many different arm-maneuvering trajectories including the two described in Sec. III.C have been checked. Two typical examples are presented in this section. In both examples, ten velocity measurements are taken at configurations equally separated along the arm's motion trajectory. The sensor error is assumed to be random with zero mean and a standard deviation defined as a percentage of the maximum velocity value. The random error is added to each of the measured velocity components. As a result, the identified inertia parameters will no longer be error free. The errors in the identified parameters will then be plotted and examined.

In example 1, the arm is commanded to go along the first trajectory defined in Sec. III.C. The spacecraft body is initially spinning about the Z axis at a rate of 1.0 deg/s. The identification errors are plotted in Fig. 13.

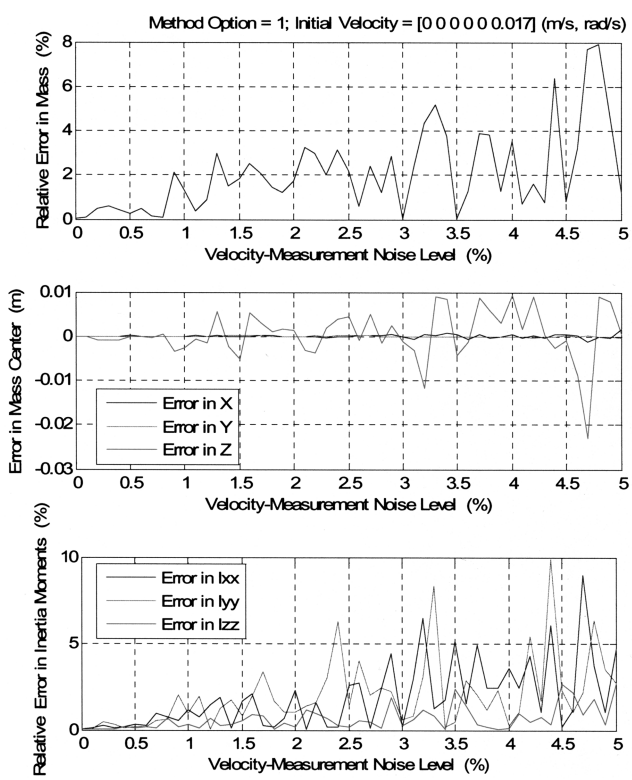

Fig. 13 Identification errors vs different noises added to the velocity data.

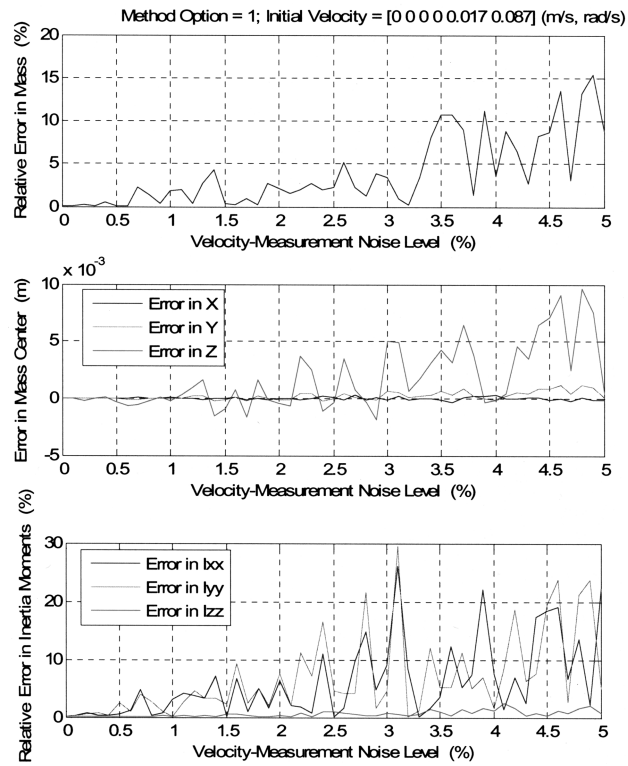

Fig. 14 Identification errors vs different noises added to the velocity data. (Note that the error in the position of the mass center is represented by the absolute error because the mass center is located at the origin, and, thus, the relative error is undefined.)

In example 2, the arm is fully stretched out and swings in the horizontal plane along the second trajectory defined in Sec. III.C. The spacecraft body is initially rotating at a rate of 1.0 deg/s about the Y axis (pitch) and 5.0 deg/s about the Z axis (yaw). The identification errors are plotted in Fig. 14.

These two examples showed that the identification along trajectory 1 can be done more accurately than that along trajectory 2. The plots clearly tell us that, if we can control the velocity-measurement errors within the 3% level, the resulting identification errors are more or less at the same level for trajectory 1. However, the same 3% measurement errors could cause over 20% identification errors if using trajectory 2. In fact, it has been generally observed that the identification errors are smaller when the arm has larger motion span. This is mainly because a larger motion span will usually have a higher signal-to-noise ratio, as already mentioned in Sec. III.C. The examples have demonstrated that a proper selection of arm maneuvering is important for the performance of the identification procedure.

The preceding examples also tell us that the errors in the identified mass and mass center are much smaller than those in the identified inertia tensor. In other words, the identification of the inertia tensor is more difficult than that of the mass and mass center because the former is more sensitive to data errors.

IV. Estimation of Identification Error

Section III presented the simulation results of the proposed identification method under the presence of velocity-measurement errors for various test scenarios. Although these numerical results give some idea of how the measurement errors affect the identification results, they do not provide a general picture of how the inevitable sensor errors affect the identification method. There is a good discussion in [18] on the pros and cons of numerical-error analysis vs analytical-error analysis. In this section we will provide a scheme for quantitatively estimating the identification-error bounds in term of the velocity-measurement errors.

A. General Scheme for Error Estimation

As described in Sec. II, our parameter identification problem is formulated as the least-squares solution to a system of linear equations as follows:

$$\mathbf{A}\mathbf{x} = \mathbf{b} \tag{29}$$

where $\mathbf{x}$ is the set of unknown inertia parameters to be identified; matrices $\mathbf{A}$ and $\mathbf{b}$ are dependent on the linear and angular velocity-measurement data $\mathbf{v}$ and $\boldsymbol{\omega}$. If the required velocity measurements are perfect without error, $\mathbf{A}$ and $\mathbf{b}$ are also perfect, and the solution $\mathbf{x}$ should be the true values of the sought parameters. However, with the presence of measurement errors in $\mathbf{v}$ and $\boldsymbol{\omega}$, namely $\Delta\mathbf{v}$ and $\Delta\boldsymbol{\omega}$, respectively, then Eq. (29) becomes

$$\tilde{\mathbf{A}}\,\tilde{x} = \tilde{\mathbf{b}} \tag{30}$$

where

$$\tilde{\mathbf{A}} = \mathbf{A} + \Delta\mathbf{A}, \qquad \tilde{\mathbf{b}} = \mathbf{b} + \Delta\mathbf{b} \tag{31}$$

Matrices $\Delta\mathbf{A}$ and $\Delta\mathbf{b}$ are errors of $\mathbf{A}$ and $\mathbf{b}$ caused by the measurement errors $\Delta\mathbf{v}$ and $\Delta\boldsymbol{\omega}$. $\tilde{\mathbf{x}}$ is the solution of Eq. (30), which no longer has the true values of the sought parameters. Rewrite the error matrices $\Delta\mathbf{A}$ and $\Delta\mathbf{b}$ as

$$\Delta\mathbf{A} = \varepsilon_A \mathbf{E}_A, \qquad \Delta\mathbf{b} = \varepsilon_b \mathbf{e}_b \tag{32}$$

where

$$\varepsilon_A = \|\Delta\mathbf{A}\|, \qquad \varepsilon_b = \|\Delta\mathbf{b}\|, \qquad \|\mathbf{E}_A\| = \|\mathbf{e}_b\| = 1 \tag{33}$$

Let the error in the identified parameters be

$$\delta\mathbf{x} = \tilde{\mathbf{x}} - \mathbf{x} \tag{34}$$

Then, the upper bound of the error in the identified parameters can be estimated by

$$\|\delta\mathbf{x}\| \le \|\mathbf{A}^+\|^2\|\mathbf{r}\|\varepsilon_A + \|\mathbf{A}^+\|(\|\mathbf{x}\|\varepsilon_A + \varepsilon_b) + N_{1\varepsilon} \tag{35}$$

and the upper bound of the relative error in the identified parameters is

$$\frac{\|\delta\mathbf{x}\|}{\|\mathbf{x}\|} \le (\kappa(\mathbf{A}))^2 \frac{\varepsilon_A}{\|\mathbf{A}\|}\zeta + \kappa(\mathbf{A})\left(\frac{\varepsilon_A}{\|\mathbf{A}\|} + \frac{\varepsilon_b}{\|\mathbf{b}\|}\gamma\right) + N_{2\varepsilon} \tag{36}$$

where $\mathbf{A}^+$ is the Moore–Penrose generalized inverse of matrix $\mathbf{A}$; $\mathbf{r}$ is the residual vector, and κ is the condition number of matrix $\mathbf{A}$. They and others are defined as

$$\mathbf{A}^+ = (\mathbf{A}^T\mathbf{A})^{-1}\mathbf{A}^{\mathbf{T}}, \qquad \mathbf{r} = \mathbf{b} - \mathbf{A}\mathbf{x}, \qquad \kappa(\mathbf{A}) = \|\mathbf{A}\|\|\mathbf{A}^+\|$$
$$\zeta = \frac{\|\mathbf{r}\|}{\|\mathbf{A}\|\cdot\|\mathbf{x}\|}, \qquad \gamma = \frac{\|\mathbf{b}\|}{\|\mathbf{A}\|\cdot\|\mathbf{x}\|} \tag{37}$$

The terms $N_{1\varepsilon}$ and $N_{2\varepsilon}$ represent the second- and higher-order terms of ε, which can be practically ignored. The reader is referred to [18–20] for the detailed discussions of the preceding error-analysis theory.

To complete the error-bound estimation, we need to calculate the error matrices $\Delta\mathbf{A}$ and $\Delta\mathbf{b}$ in terms of the velocity-measurement errors $\Delta\mathbf{v}$ and $\Delta\boldsymbol{\omega}$, which will be discussed in the next two subsections. We only consider the case when the initial linear momentum $\mathbf{p}_C(0)$ and the initial angular momentum $\mathbf{h}_C(0)$ are known (i.e., option 1 of step 1 and step 2 of the proposed identification method). The procedure is identical for option 2, when $\mathbf{p}_C(0)$ and $\mathbf{h}_C(0)$ are unknown.

B. Step 1 (Option 1): Identification of Mass and Position of Mass Center

In this case, the identification problem is represented by Eq. (11), which has exactly the same symbolic form as Eq. (29). Based on Eq. (13), we know that matrix $\tilde{\mathbf{A}}$ is related to the measured velocity data $\tilde{\boldsymbol{\omega}}_S = \boldsymbol{\omega}_S + \Delta\boldsymbol{\omega}_S$ and $\tilde{\mathbf{v}}_S = \mathbf{v}_S + \Delta\mathbf{v}_S$ as follows:

$$\tilde{\mathbf{A}}(\tilde{\boldsymbol{\omega}}_S, \tilde{\mathbf{v}}_S) = \left[\left(\tilde{\mathbf{v}}_S + \tilde{\boldsymbol{\omega}}_S \times \boldsymbol{\rho}_R - \frac{\mathbf{p}_C(0)}{m_R}\right)\tilde{\boldsymbol{\Omega}}\right] \tag{38}$$

Thus,

$$\begin{aligned}\boldsymbol{\Delta}\mathbf{A} &= \tilde{\mathbf{A}}(\boldsymbol{\omega}_S + \boldsymbol{\Delta}\boldsymbol{\omega}_S, \mathbf{v}_S + \boldsymbol{\Delta}\mathbf{v}_S) - \mathbf{A}(\boldsymbol{\omega}_S, \mathbf{v}_S) = [\,\boldsymbol{\Delta}\mathbf{v}_S + \boldsymbol{\Delta}\boldsymbol{\omega}_S \times \boldsymbol{\rho}_R \quad \boldsymbol{\Delta}\boldsymbol{\omega}_S\times\,] \\ &= \left[\begin{bmatrix} \Delta v_S(1) + \Delta\omega_S(2)\cdot\rho_R(3) - \Delta\omega_S(3)\cdot\rho_R(2) \\ \Delta v_S(2) + \Delta\omega_S(1)\cdot\rho_R(3) - \Delta\omega_S(3)\cdot\rho_R(1) \\ \Delta v_S(3) + \Delta\omega_S(1)\cdot\rho_R(2) - \Delta\omega_S(2)\cdot\rho_R(1) \end{bmatrix}\begin{bmatrix} 0 & -\Delta\omega_S(3) & \Delta\omega_S(2) \\ \Delta\omega_S(3) & 0 & -\Delta\omega_S(1) \\ -\Delta\omega_S(2) & \Delta\omega_S(1) & 0 \end{bmatrix}\right]\end{aligned} \tag{39}$$

Also from Eq. (13), $\tilde{\mathbf{b}}$ can be written as a function of $\tilde{\mathbf{v}}_S = \mathbf{v}_S + \Delta\mathbf{v}_S$:

$$\tilde{\mathbf{b}}(\tilde{\mathbf{v}}_S) = -\tilde{\mathbf{v}}_S \tag{40}$$

Therefore

$$\boldsymbol{\Delta}\mathbf{b} = \tilde{\mathbf{b}}(\mathbf{v}_S + \boldsymbol{\Delta}\mathbf{v}_S) - \mathbf{b}(\mathbf{v}_S) = -\boldsymbol{\Delta}\mathbf{v}_S = \begin{bmatrix} -\Delta v_S(1) \\ -\Delta v_S(2) \\ -\Delta v_S(3) \end{bmatrix} \tag{41}$$

C. Step 2 (Option 1): Identification of Inertia Tensor

In this case, the identification problem is represented by Eq. (18), which is still the same as Eq. (29) although different symbols are used. Based on Eq. (20), we know that matrix $\tilde{\mathbf{B}}$ is related to the measured velocity data $\tilde{\boldsymbol{\omega}}_S = \boldsymbol{\omega}_S + \Delta\boldsymbol{\omega}_S$ as follows:

$$\tilde{\mathbf{B}}(\tilde{\boldsymbol{\omega}}_S) = \begin{bmatrix} \tilde{\omega}_S(1) & 0 & 0 & \tilde{\omega}_S(2) & \tilde{\omega}_S(3) & 0 \\ 0 & \tilde{\omega}_S(2) & 0 & \tilde{\omega}_S(1) & 0 & \tilde{\omega}_S(3) \\ 0 & 0 & \tilde{\omega}_S(3) & 0 & \tilde{\omega}_S(1) & \tilde{\omega}_S(2) \end{bmatrix} \tag{42}$$

Therefore

$$\begin{aligned}\Delta\mathbf{B} &= \tilde{\mathbf{B}}(\boldsymbol{\omega}_S + \Delta\boldsymbol{\omega}_S) - \mathbf{B}(\boldsymbol{\omega}_S) \\ &= \begin{bmatrix} \Delta\omega_S(1) & 0 & 0 & \Delta\omega_S(2) & \Delta\omega_S(3) & 0 \\ 0 & \Delta\omega_S(2) & 0 & \Delta\omega_S(1) & 0 & \Delta\omega_S(3) \\ 0 & 0 & \Delta\omega_S(3) & 0 & \Delta\omega_S(1) & \Delta\omega_S(2) \end{bmatrix}\end{aligned} \tag{43}$$

Also from Eq. (20), $\tilde{\mathbf{c}}$ can be written as a function of $\tilde{\boldsymbol{\omega}}_S$:

$$\tilde{\mathbf{c}}(\tilde{\boldsymbol{\omega}}_S) = \mathbf{h}_C(0) - \mathbf{I}_R\tilde{\boldsymbol{\omega}}_S - \frac{m_R m_S}{m_S + m_R}(\boldsymbol{\rho}_S - \boldsymbol{\rho}_R) \times [\tilde{\boldsymbol{\omega}}_S \times (\boldsymbol{\rho}_S - \boldsymbol{\rho}_R)] \tag{44}$$

Therefore

$$\begin{aligned}\boldsymbol{\Delta}\mathbf{c} &= \tilde{\mathbf{c}}(\boldsymbol{\omega}_S + \boldsymbol{\Delta}\boldsymbol{\omega}_S) - \mathbf{c}(\boldsymbol{\omega}_S) \\ &= -\mathbf{I}_R\boldsymbol{\Delta}\boldsymbol{\omega}_S - \frac{m_R m_S}{m_S + m_R}(\boldsymbol{\rho}_S - \boldsymbol{\rho}_R) \times [\boldsymbol{\Delta}\boldsymbol{\omega}_S \times (\boldsymbol{\rho}_S - \boldsymbol{\rho}_R)]\end{aligned} \tag{45}$$

V. Conclusions

This paper describes a robotics-based method for on-orbit identification of the inertia properties of spacecraft. The method makes use of an onboard robotic arm to change the inertia distribution of the spacecraft system (consisting of the spacecraft and the robotic arm). As a result of the inertia redistribution, the velocity of the spacecraft will change correspondingly. Because the spacecraft velocity is measurable and the inertia redistribution of the robotic arm is precisely computable, the inertia parameters of the spacecraft become the only unknowns in the momentum equations of the spacecraft system and, hence, can be identified. To treat the problem as a linear identification problem, which is much easier to solve, a two-step procedure is introduced. The first step is to identify the mass and mass center of the spacecraft, and the second step is to identify the inertia tensor of the spacecraft. The paper also presented error-analysis schemes that can be used to estimate the upper bounds of identification errors in terms of given velocity-measurement errors.

The paper has discussed the advantages of the method, which are

1) It does not consume fuel because an onboard robotic system is energized by solar power.

2) It requires measuring velocities only, which can be done much more easily than measuring accelerations and forces.

3) Because it is momentum-based method, the identification results will not be affected by internal forces, which are very difficult to accurately measure.

The paper also presented a simulation-based study to demonstrate the feasibility of the proposed method. Simulation tests showed that the spacecraft does not require an initial spin (or rotation) for identifying the mass and mass center. However, it requires an initial spin (or rotation) to identify the inertia tensor. This initial angular momentum of the system can be unknown. Simulation results revealed that, when using a robotic arm for inertia identification, the arm mass should be no less than 5% of the spacecraft mass to obtain a good identification result. The study also revealed that the arm maneuvering for identification should have as large of a motion span as possible. However, the arm does not necessarily need 6 degrees of freedom, although more degrees of freedom can offer better maneuvering that can improve the identification results. The study also showed that, if the spacecraft initially rotates about 1 axis only, then the arm rotation should span at least 2 axes. If the spacecraft initially rotates in 2 axes, the required arm motion can span only 1 axis. The study further revealed that the identification method is insensitive to sensor noise for identifying the mass and mass-center location but very sensitive to sensor noise for identifying the inertia tensor.

Acknowledgments

This work was supported by the U.S. Air Force Research Laboratory (AFRL), Space Vehicles Directorate, through the Air Force Office of Scientific Research grant number FA9550-06-1-0284. Many helpful technical discussions with Lawrence Robertson and Benjamin Henderson of the AFRL are highly acknowledged.

References

[1] Kasai, T., Oda, M., and Suzuki, T., "Results of the ETS-7 Mission—Rendezvous Docking and Space Robotics Experiment," *5th International Symposium on Artificial Intelligence, Robotics and Automation in Space*, European Space Research and Technology Centre, Noordwijk, The Netherlands, 1999, pp. 299–306.

[2] Stamm, S., and Motaghedi, P., "Orbital Express Capture System: Concept to Reality," *Spacecraft Platforms and Infrastructure*, Proceedings of SPIE, Vol. 5419, International Society for Optical Engineering, Bellingham, WA, 2004, pp. 78–91.

[3] Bosse, A. B., Barnds, W. J., Brown, M. A., Creamer, N. G., Feerst, A., Henshaw, C. G., Hope, A. S., Kelm, B. E., Klein, P. A., Pipitone, F., Plourde, B. E., and Whalen, B. P., "SUMO: Spacecraft for the Universal Modification of Orbits," *Proceedings of SPIE*, Vol. 5419, International Society for Optical Engineering, Bellingham, WA, Apr. 2004, pp. 36–46.

[4] Hirzinger, G., Landzettel, K., Brunner, B., Fischer, M., Pruesche, C,, Reintsema, D., Albu-Schäffer, A. Schreiber, G., and Steinmetz, B.-M., "DLR's Robotics Technologies for On-Orbit Servicing," *Advanced Robotics*, Vol. 18, No. 2, 2004, pp. 139–174. doi:10.1163/156855304322758006

[5] Dupris, E., Doyon, M., Martin, E., Allard, P., Piedboeuf, J. C., and Ma, O., "Autonomous Operations for Space Robots," International Astronautical Congress, 55th International Astronautical Congress, Paper 04-IAA.U.5.03, Vancouver, 4–8 Oct. 2004.

[6] Liang, B., Li, C., Xue, L., and Qiang, W., "A Chinese Small Intelligent Space Robotic System for On-Orbit Servicing," *International Conference on Intelligent Robots and Systems*, Inst. of Electrical and Electronics Engineers, New York, Oct. 2006, pp. 4602–4607.

[7] Bergmann, E. V., Walker, B. K., and Levy, D. R., "Mass Property Estimation for Control of Asymmetrical Satellites," *Journal of Guidance, Control, and Dynamics*, Vol. 10, No. 5, 1987, pp. 483–491. doi:10.2514/3.20243

[8] Richfield, R. F., Walker, B. K., and Bergmann, E. V., "Input Selection and Convergence Testing for a Second Order Mass Property Estimator," *Journal of Guidance, Control, and Dynamics*, Vol. 11, No. 3, 1988, pp. 207–212. doi:10.2514/3.20295

[9] Bergmann, E. V., and Dzielski, J., "Spacecraft Mass Property Identification with Torque-Generating Control," *Journal of Guidance, Control, and Dynamics*, Vol. 13, No. 1, 1990, pp. 99–103. doi:10.2514/3.20522

[10] Palimaka, J., and Burlton, B.V., "Estimation of Spacecraft Mass Properties Using Angular Rate Gyro Data," *AIAA/AAS Astrodynamics Conference*, Aug. 1992, pp. 21–26.

[11] Tanygin, S., and Williams, T., "Mass Property Estimation Using Coasting Maneuvering," *Journal of Guidance, Control, and Dynamics*, Vol. 20, No. 4, 1997, pp. 625–632.

[12] Wilson, E., Lages, C., and Mah, R., "On-Line, Gyro-Based, Mass-Property Identification for Thruster-Controlled Spacecraft Using Recursive Least Squares," *45th Midwest Symposium on Circuits and Systems*, Vol. 2, Inst. of Electrical and Electronics Engineers, New York, Aug. 2002, pp. 334–337.

[13] Peck, M. A., "Mass-Properties Estimation for Spacecraft with Powerful Damping," AIAA/AAS Astrodynamics Specialist Conference, Girdwood, AK, American Astronautical Society Paper 99-430, 16–19 Aug. 1999.

[14] Ma, O., and Horan, S., "NMSU Nanosatellite with Robotics Capabilities," *8th International Symposium on Artificial Intelligence, Robotics and Automation in Space*, European Space Research and Technology Centre, Noordwijk, The Netherlands, Sept. 2005, pp. 145–148.

[15] Murotsu, Y., Senda, K., Ozaki, M., and Tsujio, S., "Parameter Identification of Unknown Object Handled by Free-Flying Space Robot," *Journal of Guidance, Control, and Dynamics*, Vol. 17, No. 3, 1994, pp. 488–494. doi:10.2514/3.21225

[16] Yoshida, K., and Abiko, S., "Inertia Parameter Identification for a Free-Flying Space Robot," AIAA Guidance, Navigation, and Control Conference, AIAA Paper 2002-4568, Monterey, CA, Aug. 2002.

[17] Angeles, J., *Fundamentals of Robotic Mechanical Systems: Theory, Methods, and Algorithms*, 3rd ed., Springer–Verlag, New York, 2006.

[18] Chatterjee, S., *Sensitivity Analysis in Linear Regression*, Wiley, New York, 1988, pp. 245–263.

[19] Elden, L., "Perturbation Theory for the Least Squares Problem with Linear Equality Constraints," *SIAM Journal on Numerical Analysis*, Vol. 17, No. 3, June 1980, pp. 338–350. doi:10.1137/0717028

[20] Fuller, W. A., *Measurement Error Models*, Wiley, New York, 1987.